Ceramics International xxx (xxxx) xxx

Contents lists available at ScienceDirect

Ceramics International

journal homepage: www.elsevier.com/locate/ceramint

Preparation, structure and microwave dielectric properties of novel La_2MgGeO_6 ceramics with hexagonal structure and adjustment of its τ_f value

Xianjie Zhou, Kangguo Wang, Sang Hu, Xiaowen Luan, Sen He, Xi Wang, Shicheng Zhou, Xiuli Chen *, Huanfu Zhou **

Guangxi Ministry-Province Jointly-Constructed Cultivation Base for State Key Laboratory of Processing for Non-ferrous Metal and Featured Materials, Guangxi Key Laboratory in Collaborative Innovation Center for Exploration of Hidden Nonferrous Metal Deposits and Development of New Materials in Guangxi, School of Materials Science and Engineering, Guilin University of Technology, Guilin, 541004, China

ARTICLE INFO

Keywords:
Ceramics
Microwave dielectric properties
La_2MgGeO_6

ABSTRACT

A novel La_2MgGeO_6 ceramic was synthesized through a solid-state reaction process within a sintering temperature range of 1450–1550 °C. By a combination of X-ray diffraction and Rietveld refinement analyses, the ceramics were found to have a pure hexagonal phase structure belonging to space group R3/146. The scanning electron microscopy images revealed that the ceramic grains were closely connected. The effects of internal (lattice energy, valence bond, and fraction packing) and external factors (density) on the microwave properties of ceramics were also studied. The ceramic exhibited excellent microwave dielectric performances, with a relative permittivity ($\mathcal{E}_r$) of 21.2, a quality factor ($Q \times f$) of 52 360 GHz, and a temperature coefficient of resonant frequency (τ_f) of −44.2 ppm/°C, when sintered at 1500 °C for 4 h. The τ_f value of the La_2MgGeO_6 ceramic doped with $CaTiO_3$ could be adjusted to zero. Particularly, $0.2La_2MgGeO_6$-$0.8CaTiO_3$ ceramics have good microwave dielectric properties with $\tau_f = +2.1$ ppm/°C, $Q \times f = 15\,610$ GHz, and $\mathcal{E}_r = 40.3$.

1. Introduction

Microwave dielectric ceramics have been used as key information materials in various fields, such as resonators, filters, and oscillators [1–3]. In commercial applications, ceramics must satisfy three basic conditions to qualify as microwave dielectric materials. (1) An appropriate relative dielectric constant which directly affects the speed of signal transmission, and is obtained via the formula: $t_d = \sqrt{\varepsilon_r}\, l_c/c$, where t_d, $\mathcal{E}_r$, l_c, and c are the signal delay time, relative permittivity, transmission distance, and velocity of light, respectively [4,5]. A high dielectric constant is beneficial to the miniaturization of devices ($\lambda = \frac{\lambda_0}{\sqrt{\varepsilon_r}}$, where λ and λ_0 are the wavelengths of the electromagnetic wave in the dielectric material and free space, respectively) [6,7]. (2) High quality factor ($Q \times f$) values that allow for frequency selectivity and enhancement of signal to noise ratio. (3) The values (~0) of resonant frequency (τ_f) should maintain stability over a particular temperature range [8–11].

Many ceramics, including $Ba(Mg_{1/3}Ta_{2/3})O_3$, $MgTiO_3$–$CaTiO_3$, and (Ca, Sm) (Al, Ti)O_4, exhibit good microwave dielectric performances, indicating the commercial applicability of these materials [12]. Rare-earth-based microwave dielectric ceramics have excellent properties, and thus attract considerable research attention from a wide range of fields. $SmAlO_3$ ceramics showed outstanding microwave dielectric properties: $\mathcal{E}_r$ ~20.4 and $Q \times f$ ~65 000 GHz [13]. $SmNbO_4$ ceramics exhibited superior microwave dielectric properties: $\mathcal{E}_r$ of 18.8 and $Q \times f$ of 56 300 GHz [14]. Ln $(Mg_{1/2}Ti_{1/2})O_3$ (Ln = Dy, La, Nd, Pr, Sm, and Y) ceramics, with perovskite-like structures, have been reported used as substrates for high-Tc superconductor thin films. Among these lanthanide-based ceramics, the $La(Mg_{1/2}Ti_{1/2})O_3$ ceramics exhibited remarkable microwave dielectric performance: $\mathcal{E}_r \approx 29$, $Q \approx 7550$, and $\tau_f \approx -65$ ppm/°C [15]. However, the La_2MgGeO_6 ceramics were neglected in the $La_2Mg\mathit{M}^{4+}O_6$ family. Ti and Ge atoms have similar radii, such that Ti was easily replaced by Ge.

In this study, the La_2MgGeO_6 ceramics were synthesized using a solid-state reaction process. The ceramics were found to be structurally

* Corresponding author.
** Corresponding author.
E-mail addresses: cxlnwpu@163.com (X. Chen), zhouhuanfu@163.com (H. Zhou).

https://doi.org/10.1016/j.ceramint.2020.11.123
Received 18 September 2020; Received in revised form 11 November 2020; Accepted 16 November 2020
Available online 19 November 2020

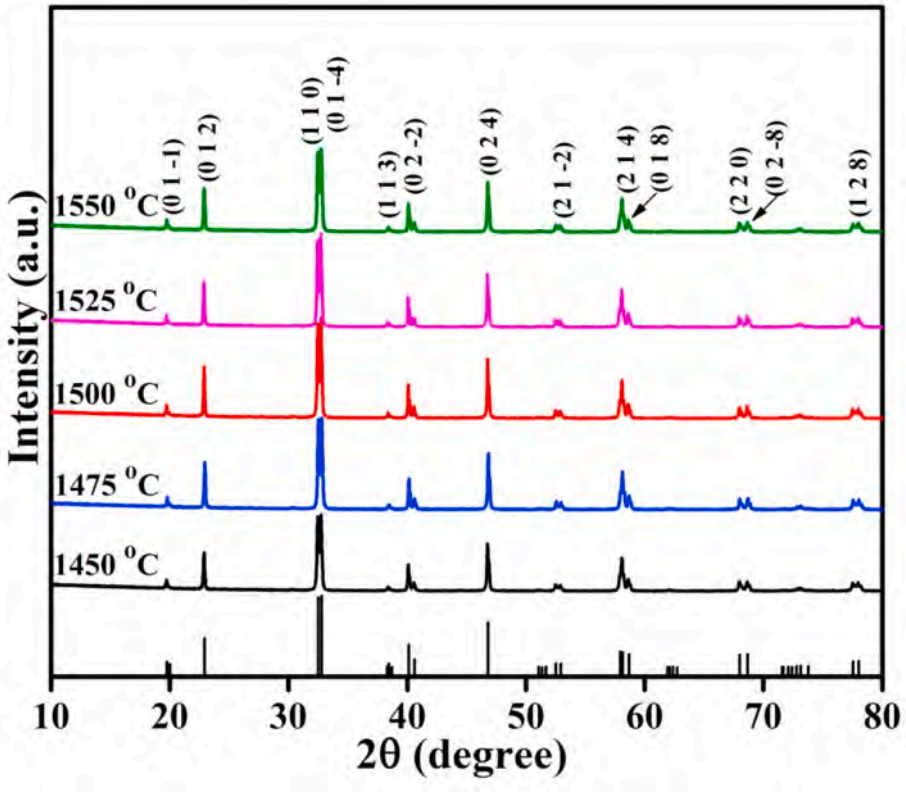

Fig. 1. XRD patterns of La_2MgGeO_6 ceramics sintered at different temperatures.

Table 1
Refinement parameters of La_2MgGeO_6 ceramics sintered at different temperatures.

S.T (°C)	Lattice Parameters (Å)		V_{unite} (Å^3)	Reliability factors		
	a = b(Å)	c(Å)		R_{wp} (%)	R_p (%)	χ^2
1450	5.5226	13.3337	352.1830	4.9	3.3	7.4
1475	5.5140	13.3304	351.0001	4.8	2.9	5.9
1500	5.5119	13.3282	350.6749	4.5	2.8	5.5
1525	5.5169	13.3311	351.3879	4.7	3.1	6.1
1550	5.5208	13.3329	351.9324	5.1	2.9	6.5

similar to the Ln $(Mg_{1/2}Ti_{1/2})O_3$ ceramic family. The effects of lattice energy, packing fraction, valence bond, sintering temperature, and bulk density on the performance of sample ceramics were also discussed. Then, the La_2MgGeO_6-based ceramics were obtained with near-zero τ_f value by addition of $CaTiO_3$.

2. Experimental section

The La_2MgGeO_6 ceramics were fabricated through the traditional solid-state reaction of La_2O_3 (≥99%), MgO (≥99%), and GeO_2 (≥99%), as described in our previous paper [16]. The mixed powders were calcined and sintered at 1200 °C and 1475–1550 °C, respectively, for 4 h. Other testing methods have been described in our previous paper [16].

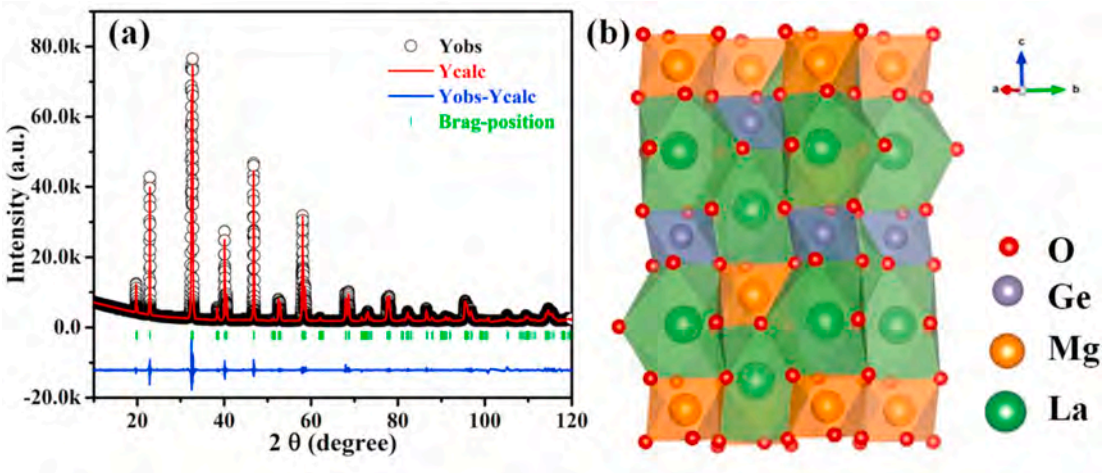

Fig. 2. Rietveld refinement and crystal structure of La_2MgGeO_6 ceramics sintered at 1500 °C.

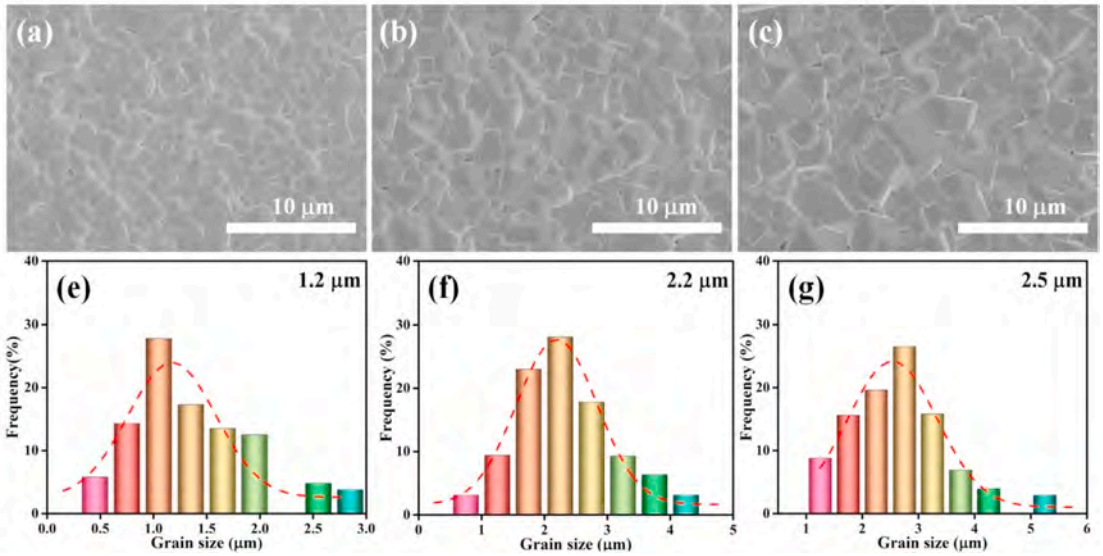

Fig. 3. SEM images of La_2MgGeO_6 ceramics sintered at: (a) 1475 °C, (b) 1500 °C, (c) 1525 °C, and grain sizes of ceramics sintered at: (d) 1475 °C, (e) 1500 °C, (f) 1525 °C.

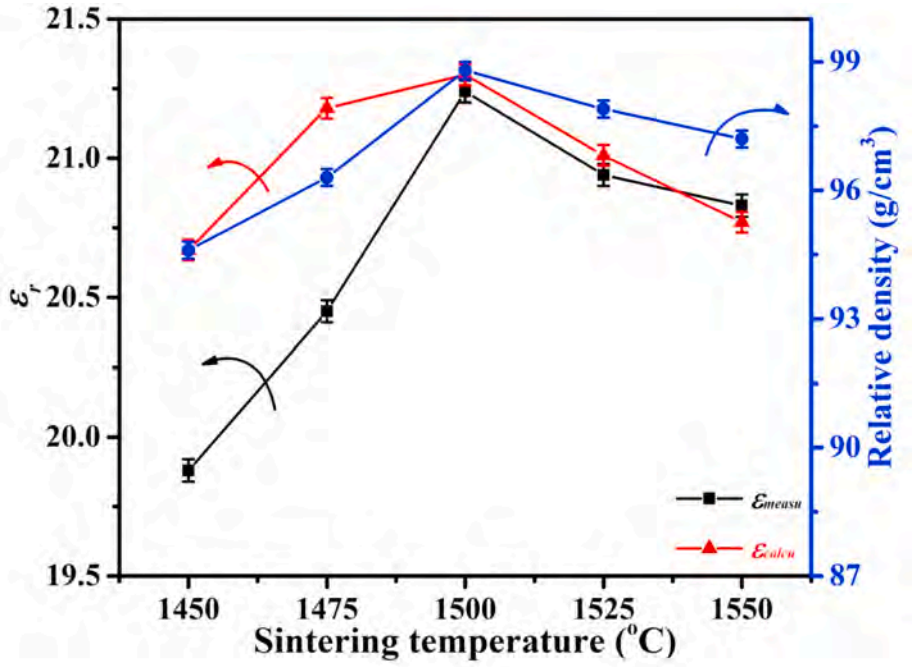

Fig. 4. ε_r and relative density of La_2MgGeO_6 ceramics as a function of sintering temperatures.

3. Results and discussion

Fig. 1 shows the X-ray diffraction (XRD) patterns of La_2MgGeO_6 ceramic powders sintered at various temperatures. The XRD pattern of ceramics sintered at 1450 °C was found to be consistent with the standard pattern of the hexagonal structure of La_2MgGeO_6, belonging to the R3/146 group (JCPDS card no. 96-711-7795), and no secondary phase was detected. On increasing the sintering temperature further to 1550 °C, the positions of the diffraction peaks remain unchanged, indicating phase structure stability of the ceramics. To determine the structure of the ceramics in detail, the XRD pattern of the ceramic sample was refined by Rietveld analysis and the refined data are presented in Table 1. The Rietveld refinements for ceramic sintered at 1500 °C are illustrated in Fig. 2(a). The values of R_p, R_w, and χ^2 were 2.8, 4.5, and 5.5, respectively, indicating that the calculated value was close to the measured one, making the refined result reliable. The ceramic structure consists of nine oxygen atoms surrounding the La atom, six oxygen atoms surrounding the Mg atom to form an [MgO_6] octahedron, and eight oxygen atoms surrounding the Ge atom to form an [GeO_6] octahedron, making up the basic framework, as shown in Fig. 2(b).

Fig. 3 illustrates the surface images and grain sizes of samples sintered at various temperatures. The ceramic grains were densely packed and had relatively fewer pores, consistent with their relatively higher density. To further increase sintering temperature, the grain size of ceramics was increased. Particularly, the La_2MgGeO_6 ceramics had equal grain size when sintered at 1500 °C, thus providing excellent performance. Fig. 4 shows the ε_r and relative density values of La_2MgGeO_6 ceramics. On increasing the sintering temperature to 1500 °C, the

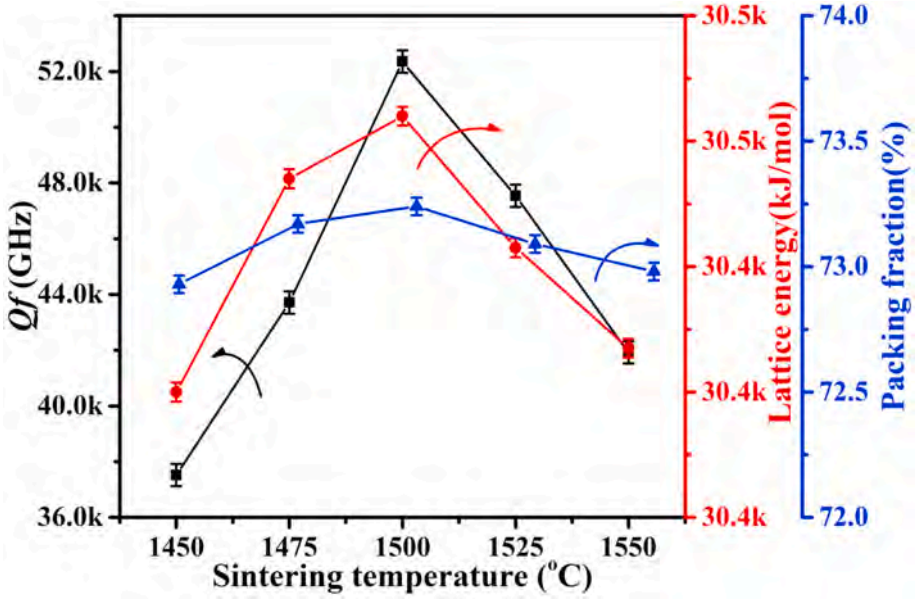

Fig. 5. $Q \times f$ values, lattice energy and packing fraction of La_2MgGeO_6 ceramics as a function of sintering temperatures.

measured ε_r values ($\varepsilon_{r\text{-}measured}$) and relative densities of the samples reached the maximum values of 21.2 and 98.6%, respectively. The trend of $\varepsilon_{r\text{-}measured}$ value corresponded with that of relative density, indicating that density significantly influences the ε_r value. ε_r also depends on other factors, such as phase structure, atomic polarization, and structural defects [17–21]. The dielectric constants of the materials were related to the polarization of the electron, which can be obtained by the following equation [22]:

$$\alpha_D = \frac{1}{b} V_m \frac{\varepsilon_r - 1}{\varepsilon_r + 2} \tag{1}$$

where α_D is the total polarizability of the substance in molar volume Vm, and $b = 4\pi/3$. In other words, the permittivity of the materials could be obtained by the following equation [19]:

$$\varepsilon_r = \frac{3V_m + 8\pi\alpha_D}{3V_m - 4\pi\alpha_D} \tag{2}$$

Shannon [23] suggested that the theoretical dielectric polarizability of La_2MgGeO_6 could be calculated as follows, using the oxide additive rule:

$$\alpha_D(La_2MgGeO_6) = 2\alpha(La^{3+}) + \alpha(Mg^{2+}) + \alpha(Ge^{4+}) + 6\alpha(O^{2-}) \tag{3}$$

Evidently, the calculated and measured ε_r values ($\varepsilon_{r\text{-}calculated}$ and $\varepsilon_{r\text{-}measured}$, respectively) show the same variation trend, indicating that the measured value had a certain degree of feasibility. The $\varepsilon_{r\text{-}calcuated}$ and $\varepsilon_{r\text{-}measrued}$ values of ceramics sintered at 1500 °C were 21.3 and 21.2, respectively. The $\varepsilon_{r\text{-}calcuated}$ value was slightly higher than the $\varepsilon_{r\text{-}measrued}$ value, indicating that other factors, such as ionic conductivity and electron conductivity, affect the dielectric constant.

Fig. 5 exhibits the $Q \times f$ values, lattice energies, and packing fraction of the samples sintered at various temperatures. In general, the dielectric losses can be categorised into internal losses, such as lattice vibrations, lattice energy, and phase structure, and external losses, such as pores, grain size, second phase, and lattice defects [24–30]. Obviously, the ceramics had a single phase and relative density exceeding 92% (Figs. 1 and 4). Therefore, the loss of the second phase and porosity in the ceramics can be disregarded. This study mainly discusses the relationship between lattice energy and the structural characteristics of ceramic losses. The structural stability is mainly reflected by the lattice energy, which can be obtained through the following formula [31]:

$$U = AI(2I/Vm)^{1/3} \tag{4}$$

$$2I = \sum_i n_i Z_i^2 \tag{5}$$

$$V_m = V_{cell}/Z \tag{6}$$

where A, I, n_i, and Z_i are the constant value ($A = 121.4$ kJ mol^{-1} nm), ionic strength, number of ions, and integral charge, respectively. The trend of lattice energy variation was consistent with that of the $Q \times f$ values of ceramics at temperatures ranging from 1450 to 1550 °C. Evidently, at a sintering temperature of 1500 °C, both the lattice energy and $Q \times f$ values reach maximum values (30 464 kJ/mol and 52 360 GHz, respectively). It was previously reported that the packing fraction was considered to directly affect the insertion loss of samples in the microwave frequency segment [32]. The structure and atomic data of ceramics were obtained from refinement analysis, and the packing fraction can be calculated using the following equation [33]:

$$\begin{aligned} Packing\ fraction &= \frac{volume\ of\ packed\ ions}{volume\ of\ primitive\ unit\ cell} \\ &= \frac{volume\ of\ \ packed\ \ ions}{volume\ of\ \ unit\ \ cell} \times Z \\ &= \frac{\frac{4\pi}{3} \times (2r_{La}^3 + r_{Mg}^3 + r_{Ge}^3 + 6r_O^3) \times 3}{volume\ of\ \ unit\ \ cell} \end{aligned} \tag{7}$$

where r_{La} (1.2 Å), r_{Mg} (0.72 Å), r_{Ge} (0.54 Å), and r_O (1.4 Å) represent the effective ionic radii of the respective elements of La_2MgGeO_6 ceramics, and $Z = 3$. Upon increasing the sintering temperature further, the change in packing fraction was consistent with that in the $Q \times f$ values of La_2MgGeO_6 ceramics, which increased initially and then decreased. When sintered at 1500 °C, The $Q \times f$ values and packing fraction of ceramic reached maximum values of 52 360 GHz and 73.24%, respectively.

The τ_f value is related to the distortion of the oxygen octahedron [34]. The [MgO_6] oxygen octahedron of La_2MgGeO_6 ceramics has two different bond lengths. Therefore, the distortion of the oxygen octahedron can be associated with the Mg-site bond valence [20], which can be obtained through the following equations [35]:

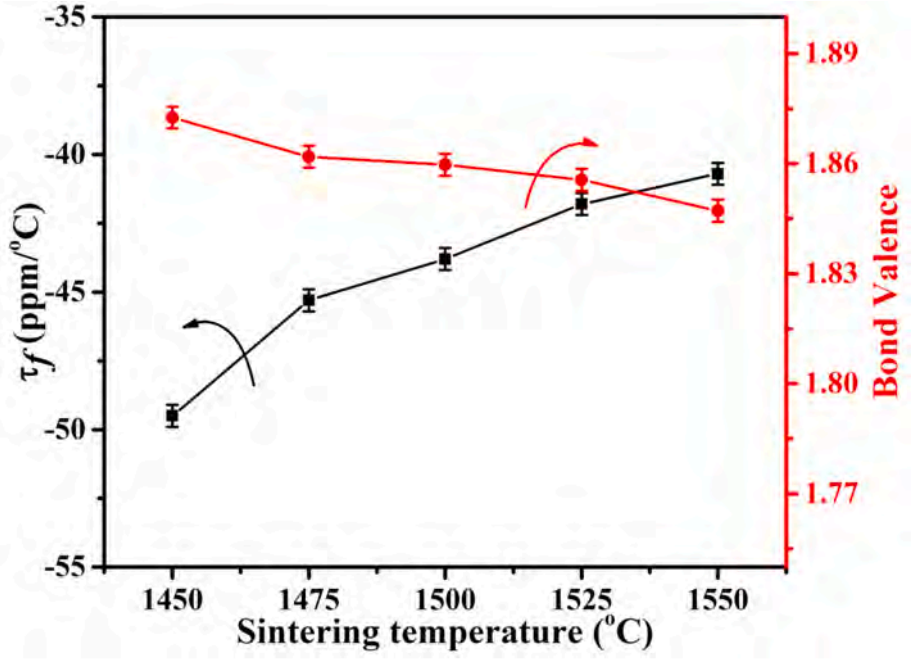

Fig. 6. τ_f values and Mg-site bond valence of La_2MgGeO_6 ceramics as a function of sintering temperatures.

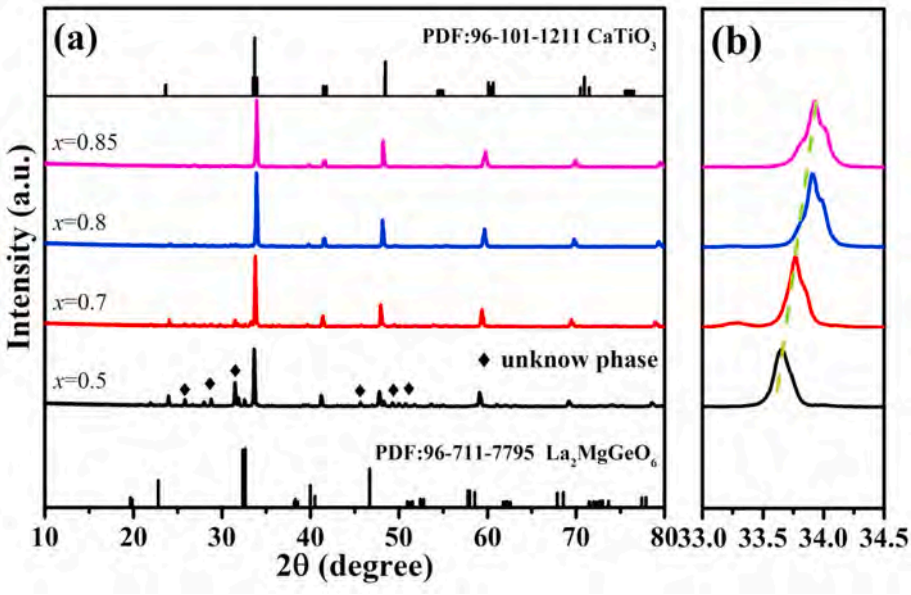

Fig. 7. XRD patterns of xCaTiO$_3$-(1-x)La$_2$MgGeO$_6$ ceramics sintered at 1500 °C.

$$V_{ij} = \sum v_{ij} \tag{8}$$

$$v_{ij} = \exp\left(\frac{R_{ij} - d_{ij}}{b'}\right) \tag{9}$$

where R_{ij}, d_{ij}, and b' are the bond valence parameter, the bond length between atoms i and j, and a universal constant (0.37 Å). Theτ_f and Mg-site bond valence of La_2MgGeO_6 ceramics sintered at various temperatures are shown in Fig. 6. At sintering temperatures ranging from 1450 to 1550 °C, the τ_f gradually increased, while the Mg-site bond valence decreased. The La_2MgGeO_6 ceramics have excellent $Q \times f$ value, but their slightly higher τ_f value limits their widespread application. The $CaTiO_3$ ceramics yielded a large τ_f value (+850 ppm/°C). Therefore, $CaTiO_3$ was added to La_2MgGeO_6 ceramics to adjust the τ_f value to zero.

Fig. 7 exhibits the XRD patterns of xCaTiO$_3$-(1-x)La$_2$MgGeO$_6$ ceramics sintered at 1500 °C. Apparently, the heterophase in the samples decreased with increasing $CaTiO_3$ content increased, and the diffraction peak inclined toward the peak type and position of $CaTiO_3$. The position of the main peak shifts to large diffraction angles with increasing $CaTiO_3$ content, as shown in Fig. 7(b). Clearly, a small amount of La_2MgGeO_6 ceramics can form a solid solution with $CaTiO_3$. Nevertheless, when the La_2MgGeO_6 ceramics content exceeded a certain amount, a hybrid phase appeared. Fig. 8 shows the scanning electron microscopy images of xCaTiO$_3$-(1-x)La$_2$MgGeO$_6$ ceramics sintered at 1500 °C. With increasing $CaTiO_3$ content, the grain shape became more uniform, confirming the results of XRD analysis. With increasing La_2MgGeO_6 content, the $CaTiO_3$ and La_2MgGeO_6 reacted to form the heterophase, leading to the appearance of grains with different shapes, as shown in Fig. 8(a). The

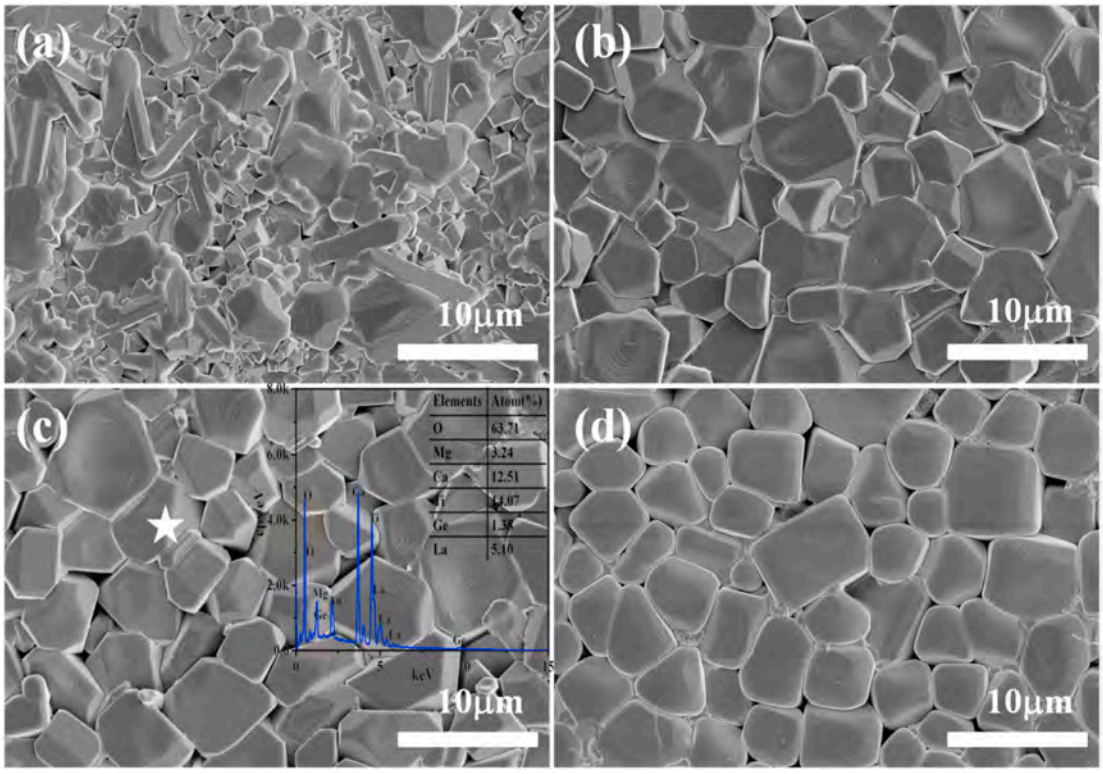

Fig. 8. SEM images of xCaTiO$_3$-(1-x)La$_2$MgGeO$_6$ ceramics sintered at 1500 °C: (a) x = 0.5, (b) x = 0.7, (c) x = 0.8, (d) x = 0.85.

Table 2
Microwave dielectric properties of xCaTiO$_3$-(1-x)La$_2$MgGeO$_6$ ceramics.

compounds	*S.T.*(°C)	ε_r	$Q\times f$ (GHz)	τ_f (ppm/°C)
La$_2$MgGeO$_6$	1500	21.2	52360	−44.2
0.5 CaTiO$_3$-0.5 La$_2$MgGeO$_6$	1500	22.9	17370	−36.8
0.7 CaTiO$_3$-0.3 La$_2$MgGeO$_6$	1500	31.5	15820	−14.7
0.8 CaTiO$_3$-0.2 La$_2$MgGeO$_6$	1500	40.3	15610	+2.1
0.85 CaTiO$_3$-0.15 La$_2$MgGeO$_6$	1500	49.2	15530	+67.2

microwave dielectric properties of xCaTiO$_3$-(1-x)La$_2$MgGeO$_6$ ceramics are presented in Table 2. With increasing CaTiO$_3$ content, the ε_r and τ_f values increased gradually, but the $Q\times f$ values initially decreased and then tended to stabilize. The τ_f (+2.1 ppm/°C) of 0.8CaTiO$_3$-0.2La$_2$MgGeO$_6$ ceramics was close to zero, but the $Q\times f$ value was drastically low.

4. Conclusion

La$_2$MgGeO$_6$ ceramics were prepared through the traditional solid-state reaction process. The XRD and Rietveld refinement analyses of the sample ceramics revealed a single-phase hexagonal structure. After sintering at 1500 °C, the ceramics exhibited compact connections and uniform grain size. The ε_r was dependent on the density and polarizability of each ion, the $Q\times f$ values were dependent on the lattice energy and the packing fraction, and the τ_f was negatively correlated with Mg-site bond valence of La$_2$MgGeO$_6$ ceramics. CaTiO$_3$ was added to La$_2$MgGeO$_6$ ceramics, and the τ_f value (+2.1) of 0.8CaTiO$_3$-0.2La$_2$MgGeO$_6$ ceramics was close to zero.

Declaration of competing interest

The authors declare that they have no known competing financial interests or personal relationships that could have appeared to influence the work reported in this paper.

Acknowledgments

This study was supported by Natural Science Foundation of China (Nos. 61761015 and 11664008), Natural Science Foundation of Guangxi (Nos. 2017GXNSFFA198011, 2018GXNSFFA050001 and 2017GXNSFDA198027), and High Level Innovation Team and Outstanding Scholar Program of Guangxi Institutes.

References

[1] Q. Lin, K. Song, B. Liu, H.B. Bafrooei, D. Zhou, W. Su, F. Shi, D. Wang, H. Lin, I. M. Reaney, Vibrational spectroscopy and microwave dielectric properties of AY$_2$Si$_3$O$_{10}$ (A=Sr, Ba) ceramics for 5G applications, Ceram. Int. 46 (2020) 1171–1177.
[2] C.J. Pei, C.D. Hou, Y. Li, G.G. Yao, Z.Y. Ren, P. Liu, H.W. Zhang, A low εr and temperature-stable Li$_3$Mg$_2$SbO$_6$ microwave dielectric ceramics, J. Alloy. Compd. 792 (2019) 46–49.
[3] X.Q. Song, K. Du, X.Z. Zhang, J. Li, W.Z. Lu, X.C. Wang, W. Lei, Crystal structure, phase composition and microwave dielectric properties of Ca$_3$MSi$_2$O$_9$ ceramics, J. Alloy. Compd. 750 (2018) 996–1002.
[4] B. Liu, C.C. Hu, Y.H. Huang, H.B. Bafrooei, K.X. Song, Crystal structure, infrared reflectivity spectra and microwave dielectric properties of CaAl$_2$O$_4$ ceramics with low permittivity, J. Alloy. Compd. 791 (2019) 1033–1037.
[5] H.F. Zhou, X.H. Tan, J. Huang, N. Wang, G.C. Fan, X.L. Chen, Phase structure, sintering behavior and adjustable microwave dielectric properties of Mg$_{1-x}$Li$_{2x}$Ti$_x$O$_{1+2x}$ solid solution ceramics, J. Alloy. Compd. 696 (2017) 1255–1259.
[6] W.S. Xia, F.Y. Yang, G.Y. Zhang, K. Han, D.C. Guo, New low-dielectric-loss NiZrNb$_2$O$_8$ ceramics for microwave application, J. Alloy. Compd. 656 (2016) 470–475.
[7] G.G. Yao, P. Liu, X.G. Zhao, J.P. Zhou, H.W. Zhang, Low-temperature sintering and microwave dielectric properties of Ca$_5$Co$_4$(VO$_4$)$_6$ ceramics, J. Eur. Ceram. Soc. 34 (2014) 2983–2987.
[8] S. Liu, B. Tang, M. Zhou, P. Zhao, Q. Xiang, X. Zhang, Z. Fang, S. Zhang, Microwave dielectric characteristics of high permittivity Ca$_{0.35}$Li$_{0.25}$Nd$_{0.35}$Ti$_{1-x}$(Zn$_{1/3}$Ta$_{2/3}$)$_x$O$_3$ ceramics (x = 0.00–0.12), Ceram. Int. 45 (2019) 8600–8606.
[9] H.F. Zhou, X.B. Liu, X.L. Chen, L. Fang, Y.L. Wang, ZnLi$_{2/3}$Ti$_{4/3}$O$_4$: a new low loss spinel microwave dielectric ceramic, J. Eur. Ceram. Soc. 32 (2012) 261–265.
[10] K.G. Wang, T.T. Yin, H.F. Zhou, X.B. Liu, J.J. Deng, S.X. Li, C.M. Lu, X.L. Chen, Bismuth borate composite microwave ceramics synthesized by different ratios of H$_3$BO$_3$ for ULTCC technology, J. Eur. Ceram. Soc. 40 (2020) 381–385.
[11] D. Zhou, L.X. Pang, D.W. Wang, Z.M. Qi, I.M. Reaney, High quality factor, ultralow sintering temperature Li$_6$B$_4$O$_9$ microwave dielectric ceramics with ultralow density for antenna substrates, ACS. Sustain. Chem. Eng. 6 (2018) 11138–11143.

[12] H.H. Guo, D. Zhou, C. Du, P.J. Wang, W.F. Liu, L.X. Pang, Q.P. Wang, J.Z. Su, C. Singh, S. Trukhanov, Temperature stable $Li_2Ti_{0.75}(Mg_{1/3}Nb_{2/3})_{0.25}O_3$-based microwave dielectric ceramics with low sintering temperature and ultra-low dielectric loss for dielectric resonator antenna applications, J. Mater. Chem. C. 8 (2020) 4690–4700.
[13] C.L. Huang, Y.C. Chen, Low temperature sintering and microwave dielectric properties of $SmAlO_3$ ceramics, Mater. Res. Bull. 37 (2002) 563–574.
[14] W.S. Xia, S.B. Zhang, T.L. Tang, Y. Wang, L.W. Shi, Enhanced quality factors of $SmNbO_4$ ceramics with MgO additive, Physica B 572 (2019) 148–152.
[15] S.Y. Cho, C.H. Kim, D.W. Kim, K.S. Honga, Dielectric properties of $Ln(Mg_{1/2}Ti_{1/2})O_3$ as substrates for high-Tc superconductor thin films, J. Mater. Res. 14 (1999) 2484–2487.
[16] X.J. Zhou, H.F. Zhou, Q. Wu, X.W. Luan, S. Hu, J.J. Deng, S.X. Li, K.G. Wang, X. L. Chen, Novel series of MLa_2WO_7(M = Sr, Ba) microwave dielectric ceramic systems with monoclinic structures, J. Mater. Sci. Mater. Electron. 31 (2020) 10819–10824.
[17] K.G. Wang, H.F. Zhou, X.B. Liu, W.D. Sun, X.L. Chen, H. Ruan, A lithium aluminium borate composite microwave dielectric ceramic with low permittivity, near-zero shrinkage, and low sintering temperature, J. Eur. Ceram. Soc. 39 (2019) 1122–1126.
[18] D. Zhou, J. Li, L.X. Pang, D.W. Wang, I.M. Reaney, Novel water insoluble $(Na_xAg_{2-x})MoO_4$ ($0 \leq x \leq 2$) microwave dielectric ceramics with spinel structure sintered at 410 degrees, J. Mater. Chem. C. 5 (2017) 6086–6091.
[19] W.B. Li, D. Zhou, D. Guo, L.X. Pang, G.H. Chen, Z.M. Qi, Q.P. Wang, H.C. Liu, Structure, Raman spectra, far-infrared spectra and microwave dielectric properties of temperature independent $CeVO_4$-TiO_2 composite ceramics, J. Alloy. Compd. 694 (2017) 40–45.
[20] H. Li, X. Chen, Q. Xiang, B. Tang, J. Lu, Y. Zou, S. Zhang, Structure, bond characteristics and Raman spectra of $CaMg_{1-x}Mn_xSi_2O_6$ microwave dielectric ceramics, Ceram. Int. 45 (2019) 14160–14166.
[21] W. Liu, R. Zuo, Low temperature fired $Ln_2Zr_3(MoO_4)_9$ (Ln=Sm, Nd) microwave dielectric ceramics, Ceram. Int. 43 (2017) 17229–17232.
[22] Z.B. Feng, C.F. Xing, J.X. Bi, X.S. Jiang, H.T. Wu, Sintering characteristics and microwave dielectric properties of low loss $CoZrNb_2O_8$ ceramics achieved by reaction sintering process, J. Alloy. Compd. 686 (2016) 923–929.
[23] W. Liu, R. Zuo, A novel low-temperature firable $La_2Zr_3(MoO_4)_9$ microwave dielectric ceramic, J. Eur. Ceram. Soc. 38 (2018) 339–342.
[24] R.D. Shannon, Dielectric polarizabilities of ions in oxides and fluorides, J. Appl. Phys. 73 (1993) 348–366.
[25] G.G. Yao, P. Liu, Zhou, H.W. Zhang, Novel series of low-firing microwave dielectric ceramics: $Ca_5A_4(VO4)_6$ (A^{2+}=Mg, Zn), J. Am. Ceram. Soc. 96 (2013) 1691–1693.
[26] H.L. Pan, Q.Q. Liu, Y.H. Zhang, H.T. Wu, Crystal structure and microwave dielectric characteristics of Co-substituted $Zn_{1-x}Co_xZrNb_2O_8$ ($0 \leq x \leq 0.1$) ceramics, RSC Adv. 6 (2016) 86889–86903.
[27] H.H. Guo, D. Zhou, L.X. Pang, Z.M. Qi, Microwave dielectric properties of low firing temperature stable scheelite structured (Ca,Bi)(Mo,V)O_4 solid solution ceramics for LTCC applications, J. Eur. Ceram. Soc. 39 (2019) 2365–2373.
[28] H. Chen, S. Zhang, B. Tang, H. Yang, M. Zhou, F. Si, E. Li, H. Wang, X. Quan, H. Li, The observation and prediction of constant quality factors of $LnAlO_3$ doped $Ba_{6-3x}Ln_{8+2x}Ti_{18}O_{54}$ (Ln = Nd, Sm, La) ceramics, Ceram. Int. 44 (2018) 4611–4614.
[29] E. Li, X. Yang, H. Yang, H. Yang, H. Sun, Y. Yuan, Zhang, Crystal structure, microwave dielectric properties and low temperature sintering of $(Al_{0.5}Nb_{0.5})^{4+}$ co-substitution for Ti^{4+} of $LiNb_{0.6}Ti_{0.5}O_3$ ceramics, Ceram. Int. 45 (2019) 5418–5424.
[30] X.Q. Song, W. Lei, Y.Y. Zhou, T. Chen, S.W. Ta, Z.X. Fu, W.Z. Lu, Ultra-low fired fluoride composite microwave dielectric ceramics and their application for $BaCuSi_2O_6$-based LTCC, J. Am. Ceram. Soc. 103 (2019) 1140–1148.
[31] M.J. Wu, Y.C. Zhang, J.D. Chen, M.Q. Xiang, Microwave dielectric properties of sol-gel derived $NiZrNb_2O_8$ ceramics, J. Alloy. Compd. 747 (2018) 394–400.
[32] Y. Zhao, P. Zhang, Preparation for ultra-low loss dielectric ceramics of $ZnZrNb_2O_8$ by reaction-sintering process, J. Alloy. Compd. 672 (2016) 630–635.
[33] Q. Dai, R. Zuo, A novel ultralow-loss Sr_2CeO_4 microwave dielectric ceramic and its property modification, J. Eur. Ceram. Soc. 39 (2019) 1132–1136.
[34] M. Xiao, Q. Gu, Z. Zhou, P. Zhang, Study of the microwave dielectric properties of $(La_{1-x}Sm_x)NbO_4$ (x=0-0.10) ceramics via bond valence and packing fraction, J. Am. Ceram. Soc. 100 (2017) 3952–3960.
[35] H.L. Pan, C.F. Xing, J.X. Bi, X.S. Jiang, Y.X. Mao, H. Wu, Sintering characteristics and microwave dielectric properties of low loss $MgZrNb_2O_8$ ceramics achieved by reaction sintering process, J. Alloy. Compd. 687 (2016) 274–279.